Bone Reports 12 (2020) 100269

Contents lists available at ScienceDirect

Bone Reports

journal homepage: www.elsevier.com/locate/bonr

Raman microspectroscopy demonstrates reduced mineralization of subchondral bone marrow lesions in knee osteoarthritis patients

Yea-Rin Lee[a,b], David M. Findlay[a], Dzenita Muratovic[a], Tiffany K. Gill[a], Julia S. Kuliwaba[a,*]

[a] Adelaide Medical School, The University of Adelaide, Adelaide, Australia
[b] School of Pharmacy and Medical Sciences, The University of South Australia, Adelaide, Australia

ARTICLE INFO

Keywords:
Knee osteoarthritis
Bone marrow lesion (BML)
Magnetic resonance imaging (MRI)
Subchondral trabecular bone
Raman spectroscopy
Bone mineralization

ABSTRACT

Introduction: Bone marrow lesions (BMLs) are frequently identified by MRI in the subchondral bone in knee osteoarthritis (KOA). BMLs are known to be closely associated with joint pain, loss of the cartilage and structural changes in the subchondral trabecular bone (SCTB). Despite this, understanding of the nature of BMLs at the trabecular tissue level is incomplete. Thus, we used Raman microspectroscopy to examine the biochemical properties of SCTB from KOA patients with presence or absence of BMLs (OA-BML, OA No-BML; respectively), in comparison with age-matched cadaveric non-symptomatic controls (Non-OA CTL).

Methods: Tibial plateau (TP) specimens were collected from 19 KOA arthroplasty patients (6-Male, 13-Female; aged 56–74 years). BMLs were identified *ex-vivo* by MRI, using PDFS- and T1-weighted sequences. The KOA specimens were then categorized into an OA-BML group (n = 12; containing a BML within the medial condyle only) and an OA No-BML group (n = 7; with no BMLs identified in the TP). The control (CTL) group consisted of Non-OA cadaveric TP samples with no BMLs and no macroscopic or microscopic evidence of OA-related changes (n = 8; 5-Male, 3-Female; aged 44–80 years). Confocal Raman microspectroscopy, with high spatial resolution, was used to quantify the biochemical properties of SCTB tissue of both the medial and the lateral condyle in each group.

Results: The ratios of peak intensity and integrated area of bone matrix mineral (Phosphate (v1), Phosphate (v2) and Phosphate (v4)), to surrogates of the organic phase of bone matrix (Amide I, Proline and Amide III), were calculated. Within the medial compartment, the mineral:organic matrix ratios were significantly lower for OA-BML, compared to Non-OA CTL. These ratios were also significantly lower for the OA-BML medial compartment, compared to the OA-BML lateral compartment. There were no group or compartmental differences for Carbonate:Phosphate (v1, v2 and v4), Amide III (α-helix):Amide III (random-coil), Hydroxyproline:Proline, or Crystallinity.

Conclusion: As measured by Raman microspectroscopy, SCTB tissue in BML zones in KOA is significantly less mineralized than the corresponding zones in individuals without OA. These data are consistent with those obtained using other methods (e.g. Fourier transform infrared spectroscopy; FTIR) and with the increased rate of bone remodeling observed in BML zones. Reduced mineralization may change the biomechanical properties of the trabecular bone in BMLs and the mechanical interaction between subchondral bone and its overlying cartilage, with potential implications for the development and progression of OA.

1. Introduction

Bone marrow lesions (BMLs) are frequently detected by MRI in the subchondral bone of patients with both early and late stage of knee osteoarthritis (KOA) (Felson et al., 2003). Although BMLs are predominantly located in the medial compartment of the knee, in the areas of known high mechanical overload (Roberts et al., 2018), the etiology of BMLs is still unknown. BMLs are clinically associated with joint pain (Felson et al., 2001; Ip et al., 2011), cartilage volume loss (Hunter et al., 2006; Raynauld et al., 2008), and structural changes within the subchondral trabecular bone (SCTB) (Driban et al., 2013), and therefore appear to have diagnostic and prognostic value in KOA.

* Corresponding author at: Discipline of Orthopaedics and Trauma, Adelaide Medical School, The University of Adelaide, Level 7, Adelaide Health and Medical Sciences Building, Corner of North Terrace and George Street, Adelaide 5000, Australia.
E-mail addresses: yea.lee@adelaide.edu.au (Y.-R. Lee), david.findlay@adelaide.edu.au (D.M. Findlay), dzenita.muratovic@adelaide.edu.au (D. Muratovic), tiffany.gill@adelaide.edu.au (T.K. Gill), julia.kuliwaba@adelaide.edu.au (J.S. Kuliwaba).

https://doi.org/10.1016/j.bonr.2020.100269
Received 6 February 2020; Accepted 6 April 2020
Available online 22 April 2020

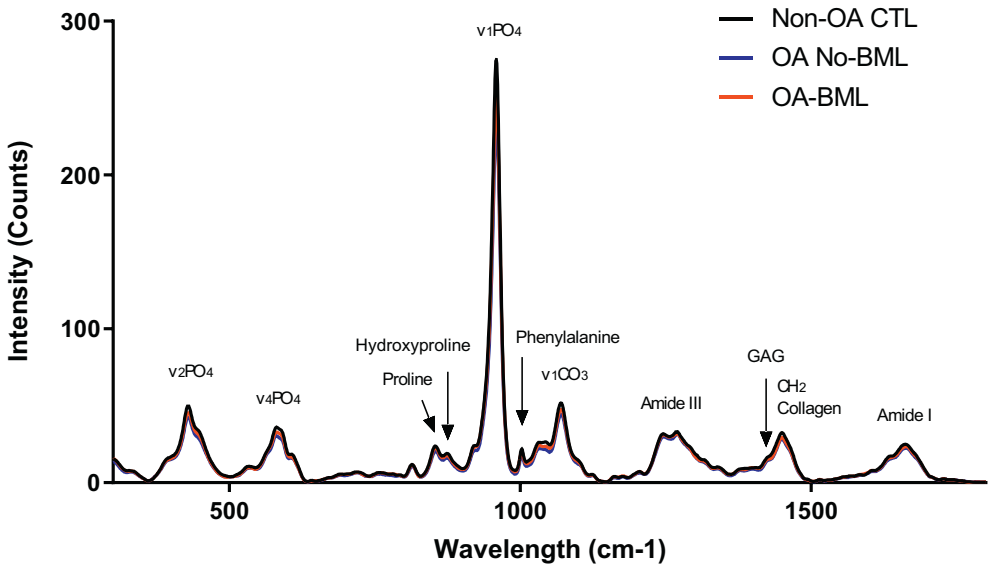

Fig. 1. Image showing the average intensity of the Raman spectra (baseline corrected, normalized) for medial SCTB tissue from all three groups (Non-OA CTL; OA No-BML and OA-BML).

Histopathological examination of the tissue that comprises BMLs has found severe bone changes, which include thicker subchondral plate, increased trabecular volume and more plate-like trabeculae, increased microdamage, and increased evidence of bone remodeling, with more eroded bone surface and increased non-mineralized osteoid volume (Muratovic et al., 2016, 2018, 2019). However, the biochemistry of the bone within BMLs has received little attention. Only a single publication reported reduced mineralization in bone cores corresponding to BMLs, when measured using micro-CT (Kazakia et al., 2013). In recent years, vibrational spectroscopy techniques, such as Raman spectroscopy (RS) (Kerns et al., 2014; Morris and Mandair, 2011; Pavlou et al., 2018) and Fourier transform infrared spectroscopy (FTIR) (Kazakia et al., 2013), have emerged as powerful assessment tools for interrogating the biochemical properties of both human and animal bone tissue.

Historically, RS was thought to be difficult to perform, however, developments in the sources such as diode lasers, charge-coupled devices (CCD), small spectrometers, and optics along with interfacing optical fibres with Raman have made it user-friendly for many analytical applications (Kuhar et al., 2018). RS is a label-free, non-invasive technique that is performed in reflection mode, meaning that it can be used to analyze a biological sample without the need to section it. The method requires minimal sample preparation and is low sensitive to the presence of water (Morris and Mandair, 2011; Pavlou et al., 2018; Butler et al., 2016; Esmonde-White, 2014). RS is, therefore, well suited to the interrogation of fresh bone samples obtained at surgery. As there are limited studies measuring the biochemical properties of human OA subchondral bone, particularly in BML zones, we applied confocal Raman microspectroscopy to interrogate the overall biochemical properties of trabecular bone tissue within BMLs. Comparisons were then made between tibial SCTB from late-stage KOA patients with and without tibial BMLs (OA-BML, OA No-BML; respectively), and age-matched cadaveric controls (Non-OA CTL) without OA and BMLs.

2. Methods

2.1. Specimen collection and MRI assessment

Tibial plateaus (TP) were obtained from 19 patients aged 56 to 74 years, of whom 6 were males (32%) and 13 were females (68%), undergoing knee arthroplasty for late-stage OA. The Non-OA group comprised n = 8 control TP, that were collected from 6 cadavers (two subjects with bilateral collection; both left and right knee), with no macroscopic or microscopic signs of KOA, aged 44 to 80 years, of whom 5 were males and 3 were females. Specimens were collected with informed written consent from all patients and with approval from the Human Research Ethics Committee at the Repatriation General Hospital, the Royal Adelaide Hospital and The University of Adelaide, South Australia, in accordance with the Declaration of Helskinki 1975. Inclusion criteria were: radiographic OA with severe symptomatic disabilities, in particular, severe pain and limited mobility. Exclusion criteria were: secondary OA of the knee due to trauma, rheumatoid arthritis, osteoporosis or evidence of bone-related chronic debilitating disease.

To identify BMLs, TP were MRI scanned (3 T MRI Siemens TRIO, Berlin, Germany) *ex-vivo*, using two specific sequences: fat-suppressed (FS) proton density-weighted sequences (PDFS) and T1-weighted sequences, as described previously (Muratovic et al., 2016, 2018, 2019). After MRI, KOA samples were categorized into an OA-BML group, in which BMLs were detected in the medial condyle (n = 12) and OA No-BML, in which no BML was detected in the TP (n = 7). None of the cadaveric (Non-OA CTL) control TP (n = 8) had any MRI evidence of BMLs.

2.2. Radiographic and cartilage assessment of OA

Radiographic evidence of OA severity was assessed according to the Kellgren and Lawrence (K&L) 0-IV scale grade, by two experienced assessors (AW and Y-YW) with 5% disagreement. Assessors were blinded to the presence of BMLs in the knee joint. All retrieved TP were also examined and graded macroscopically, according to the Outerbridge classification (Slattery and Kweon, 2018), by two orthopaedic surgeons blinded for the presence of BMLs in the tibial tissue.

Both BML and cartilage volume in mm^3 were measured directly from MRI images, using the OsiriX software (Pixmeo-SARL, Switzerland), with the manual marking and automatic volume rendering function to calculate volume. Assessors Y-RL and DM were blinded to case identity and the final scores were obtained as the average score values. The coefficient of variation for the measurement of BML volume was 2.4%, and for cartilage volume was 2.2%.

2.3. Regional sampling and tissue preparation

Blocks of tissue comprising the osteochondral unit (cartilage-

Table 1
Raman physiochemical parameters.[a]

	Peak ratio	Integrated area ratio	Assessment	Reference(s)
1. Mineral-to-matrix	Phosphate v1, v2 and v4 (~962 cm^{-1}, ~430 cm^{-1}, ~590 cm^{-1}; respectively) to Amide I (~1660 cm^{-1}), Proline (~853 cm^{-1}) and Amide III (~1242 cm^{-1})	Phosphate v1 and v2 (~959–962 cm^{-1}, ~430–450 cm^{-1}; respectively) to Amide III (~1242–1272 cm^{-1})	Bone mineralization content	Kerns et al., 2014; Buchwald et al., 2012; Nyman et al., 2011; Gamsjaeger et al., 2010; Dehring et al., 2006.
2. Carbonate-to-phosphate	Carbonate (~1076 cm^{-1}) to Phosphate v1, v2 and v4	Carbonate (~1070–1076 cm^{-1}) to phosphate v2	Carbonate substitution in the apatite crystal	Kerns et al., 2014; Buchwald et al., 2012; de Souza et al., 2012; Nyman et al., 2011; Gamsjaeger et al., 2010; Dehring et al., 2006.
3. Collagen-cross link (maturity)	Amide III (~1272 cm^{-1}) to Amide III (~1242 cm^{-1})	–	Collagen fibril maturity	Buchwald et al., 2012.
4. Hydroxyproline-to-proline	Hydroxyproline (~872 cm^{-1}) to Proline (~853 cm^{-1})	–	Collagen secondary structure	Unal et al., 2018; Buckley et al., 2012.
5. Mineral crystallinity	Full width at half maximum (FWHM) to phosphate v1	–	Crystal size and/or perfection	Lastra Luque et al., 2019; Nyman et al., 2011; Turunen et al., 2011.

[a] The above parameters were calculated on the basis of the corrected and normalized spectra.

subchondral bone), of size 10 mm × 10 mm × 5 mm, were cut from the area of BML location on the medial condyle, using a low-speed diamond wheel saw (Model 660, South Bay Technology). Lateral condyle samples, from corresponding locations, were cut into the same size blocks as a control for intragroup variability analysis. Half of the tissue block was used for RS and half was decalcified, processed, paraffin embedded, cut into 5-micron thick sections and stained by Safranin-O/Fast Green to obtain histological Osteoarthritis Research Society International (OARSI) grade (Waldstein et al., 2016). OARSI grading was performed by three assessors (Y-RL, DM and EG), blinded to the BML status of the samples and with extensive experience in quantitative histopathology. The intra-class correlation coefficient (ICC) for inter-observer reproducibility was 0.82 (95% CI 0.80, 0.84).

2.4. Raman spectroscopy

Prior to RS, lipids were removed from the tissue samples, to avoid the effect of strong light scattering on Raman that can result in lipid spectral peaks overlying some of the bone matrix spectral peaks, as previously validated by (Kerns et al., 2014), and with some modifications (Mansell and Bailey, 1998; Bachra and Fischer, 1968). Briefly, osteochondral unit tissue samples were washed in 5 ml of acetone for 1 h at room temperature by constant agitation on a roller. The samples were then rinsed several times in distilled water to remove the acetone (Kerns et al., 2014).

Spectra were acquired directly from the SCTB (~3 mm below the cartilage, if present), using a Raman microspectrometer (combines an optical microscopy and a Raman spectrometer; LabRAM High Resolution 800 (HORIBA, Jobin-Yvon, France), with DuoScan technology) which offers advanced confocal imaging capability with high performance and intuitive simplicity. This device was equipped with an XYZ motorized stage and a diode 785 nm near-infrared laser (un-polarized, to minimize the influence of polarization on band intensities (Kazanci et al., 2006; Mandair and Morris, 2015; Makowski et al., 2013), and 100% laser power was used for excitation. A continuous laser beam was focused onto a micro-meter size spot on the surface of the SCTB sample, identified through a microscope (Olympus, objective x50). Calibration was performed at the start of each session, using a silicon standard with a known Raman band at 520.5 cm^{-1}.

Five spectra, obtained directly from trabecular bone at 2 mm intervals across the entire tissue section, were collected for each sample, with an integration time of 10 s and three accumulations at each site. The spectral range was selected from 200 to 2000 cm^{-1}, with a resolution of 4 cm^{-1}. Spectra were then baseline corrected, using an automatic fitting algorithm (mixed Gaussian/Lorentzian functions) with computational Labspec6 software (HORIBA, Jobin-Yvon, France), prior to evaluation of physiochemical parameters (Fig. 1) (Penel et al., 2005; Movasaghi et al., 2007; Frushour and Koenig, 1975; Awonusi et al., 2007). The Raman instrument settings were adopted from previous published papers (Nyman et al., 2011; Imbert et al., 2014; Pascart et al., 2017) and kept constant for all measurements. Tissue samples were placed in the same positioning of the frontal axis to the microscope installed inside the Raman instrument and kept the same height distance throughout spectra acquisition to avoid any orientation effects.

The intensity of individual Raman bands (or peaks) cannot be used alone as an empirical measure of the mineral and organic components content in bone tissue, due to an irregularity of biological material, and other optical effects in bone, such as grain size, refractive index, and surface roughness of the tissue that can strongly influence the band intensity (Morris and Mandair, 2011; Mandair and Morris, 2015; Buchwald et al., 2012). It is important to take this into account in the selection of the band for the calculation of the (individual) intensity peak ratios or integrated area (under the curve) ratios. In previous studies, for example, the Phosphate; v1PO4 and the Amide I bands were strongly dependent on the orientation of the tissue (Gamsjaeger et al., 2010; Roschger et al., 2014). Thus, we also used a band that is not

Table 2
Patient demographic characteristics and cartilage assessment.

Patient demographic & cartilage assessment	Non-OA CTL (n = 8)	OA No-BML (n = 7)	OA-BML (n = 12)	p-Value
Age (years)	63.8 ± 13.8	69.6 ± 2.6	66.5 ± 5.2	0.4[a], 0.8[b], 0.7[c]
Male, number (%)	5.0 (62%)	1.0 (14%)	5.0 (42%)	0.5[a], 0.9[b], 0.4[c]
Female, number (%)	3.0 (38%)	6.0 (86%)	7.0 (58%)	0.6[a],0.4[b], 1.0[c]
BMI	24.4 (23.3, 25.0)	36.5 (28.3, 40.3)	33.6 (30.2, 39.3)	0.02[a], 0.008[b], > 1.0[c]
K&L grade	0.0 (0.0, 0.0)	2.0 (1.0, 3.0)	3.0 (3.0, 3.0)	0.007[a], 0.0005[b], > 1.0[c]
Outerbridge classification	0.0 (0.0, 0.0)	3.0 (3.0, 4.0)	4.0 (3.0, 4.0)	0.01[a], 0.0002[b], > 1.0[c]
BML medial lesion, number (%)	NA	NA	12.0 (100%)	NA
BML lateral lesion, number (%)	NA	NA	0.0 (0%)	NA
BML volume (mm^3)	NA	NA	0.4 ± 0.3	NA
Cartilage volume (mm^3), medial	1.5 ± 0.3	1.4 ± 0.3	1.1 ± 0.4	0.7[a], 0.1[b], 0.2[c]
Cartilage volume (mm^3), lateral	1.9 ± 0.1	1.5 ± 0.2	1.4 ± 0.2	0.002[a], < 0.0001[b], 0.4[c]
OARSI score, medial	0.0 (0.0, 0.0)	3.8 (1.9, 4.4)	5.5 (4.3, 5.9)	0.1[a], < 0.0001[b], 0.3[c]
OARSI score, lateral	0.9 ± 0.9	2.5 ± 0.4	2.4 ± 0.7	0.004[a], 0.004[b], 0.7[c]

Abbreviations: BMI = body mass index, K&L = Kellgren & Lawrence. Values presented as mean ± standard deviation or median (25th, 75th percentiles).
[a] Non-OA CTL *vs.* OA No-BML.
[b] Non-OA CTL *vs.* OA-BML.
[c] OA No-BML *vs.* OA-BML.

sensitive to an orientation effect, such as the Phosphate; v2PO4, v4PO4 or the Amide III band (Kazanci et al., 2006). We have reported the relative peak intensity ratios and integrated area ratios, corresponding to characteristic individual Raman bands observed in the mean spectra of each group, of select pairs of bands from the Raman spectrum, as described previously, and shown in Table 1 (Kerns et al., 2014; Nyman et al., 2011; Buchwald et al., 2012; Gamsjaeger et al., 2010; Dehring et al., 2006; de Souza et al., 2012; Unal et al., 2018; Turunen et al., 2011; Lastra Luque et al., 2019).

2.5. Statistical analysis

The patients' demographic characteristics, and cartilage and BML assessment data were either normally or non-normally distributed (Shapiro-Wilk). The group differences were calculated using analysis of variance (ANOVA). For parametric data, ANOVA and the Holm-Sidak comparison test with single pooled variance, were performed. For non-parametric data, the Kruskal-Wallis test and Dunn's multiple comparison test were performed. The statistical significance was chosen as $p < 0.05$. The analyses were performed using the GraphPad Prism 8 software (GraphPad Software, Inc., USA).

The Raman data were analyzed using the IBM SPSS for windows, version 25 (SPSS Inc.) statistics program, with analysis performed by an experienced statistician. After an initial check for normal distribution of the data (Shapiro-Wilk and Skewness and Kurtosis), and whether ANOVA is appropriate, linear regression using Generalized Estimating Equations (GEE) (with an independence working correlation) was used to model the mean of each (individual) peak ratio or integrated area (under the curve) ratio. To determine differences between groups and TP compartments, an interaction term was included in the model adjusting for clustering on subject (two possible sides, left and right knee) and controlling for age, gender and body mass index (BMI), as they are influential factors for biochemical changes in the tissue. A p-value of < 0.05 was accepted as significant.

3. Results

3.1. Patient demographics and cartilage analysis

The demographic characteristics of the individual patients, grouped according to the presence or absence of BMLs in the TP samples, are summarized in Table 2. There were no significant differences between the three groups (Non-OA CTL; OA No-BML and OA-BML) in age, gender or cartilage volume (mm^3) for the medial compartment. However, BMI, K&L grade (of the whole TP), Outerbridge classification (of the whole TP), cartilage volume (mm^3) for the lateral compartment, and OARSI histological score for the medial and lateral compartments were all significantly different between the three groups.

The median radiographic K&L and macroscopic Outerbridge classification scores were all significantly higher for OA-BML compared to Non-OA CTL ($p = 0.0005$, $p = 0.0002$; respectively), and for OA No-BML compared to Non-OA CTL ($p = 0.0066$, $p = 0.0099$; respectively) (Fig. 2). In the medial and lateral compartments, the OARSI score was significantly higher for OA-BML compared to Non-OA CTL ($p < 0.0001$, $p < 0.004$; respectively), (Fig. 2). In the lateral compartment only, the OARSI score for OA No-BML was significantly higher than Non-OA CTL. No change in cartilage volume between groups was observed for the medial compartment. However, in the lateral compartment, a reduced cartilage volume was detected in OA-BML compared to Non-OA CTL ($p < 0.0001$), and OA No-BML compared to Non-OA CTL ($p = 0.002$) (Fig. 2).

3.2. Raman assessment (peak ratios)

3.2.1. Group comparison (within compartment)

Within the medial compartment, the mineral:matrix ratios of Phosphate (v1):Amide I, Proline, Amide III; Phosphate (v2):Amide I, Proline, Amide III, and Phosphate (v4):Amide I were all significantly lower for OA-BML compared to Non-OA CTL ($p = 0.002$, $p = 0.014$, $p = 0.038$, $p = 0.004$, $p = 0.027$, $p = 0.028$, $p = 0.002$; respectively) (Fig. 3). No other group differences for the mineral:matrix ratios were observed. There were no group differences for Carbonate:Phosphate (v1, v2 and v4), Amide III (α-helix):Amide III (random-coil) (Buchwald et al., 2012), Hydroxyproline:Proline, or Crystallinity in either the medial or lateral compartments (refer to supplementary data table).

3.2.2. Medial-lateral comparisons

Comparing the medial to lateral compartments within groups, significantly lower mineral:matrix ratio of Phosphate (v1, v2 and v4):Amide I ($p = 0.018$, $p = 0.013$, $p = 0.028$; respectively) and the mineral:matrix ratio of Phosphate (v1, v2 and v4):Amide III ($p < 0.0001$, $p < 0.0001$, $p < 0.0001$, respectively), were found in the medial compartment of the OA-BML group (Fig. 4). In addition, the mineral:matrix ratio of Phosphate (v1, v2 and v4):Amide III was significantly lower in the Non-OA CTL medial compared to the Non-OA CTL lateral compartment ($p = 0.038$, $p = 0.015$, $p = 0.036$; respectively) (Fig. 4). There were no compartment differences for any other peak ratios for each group.

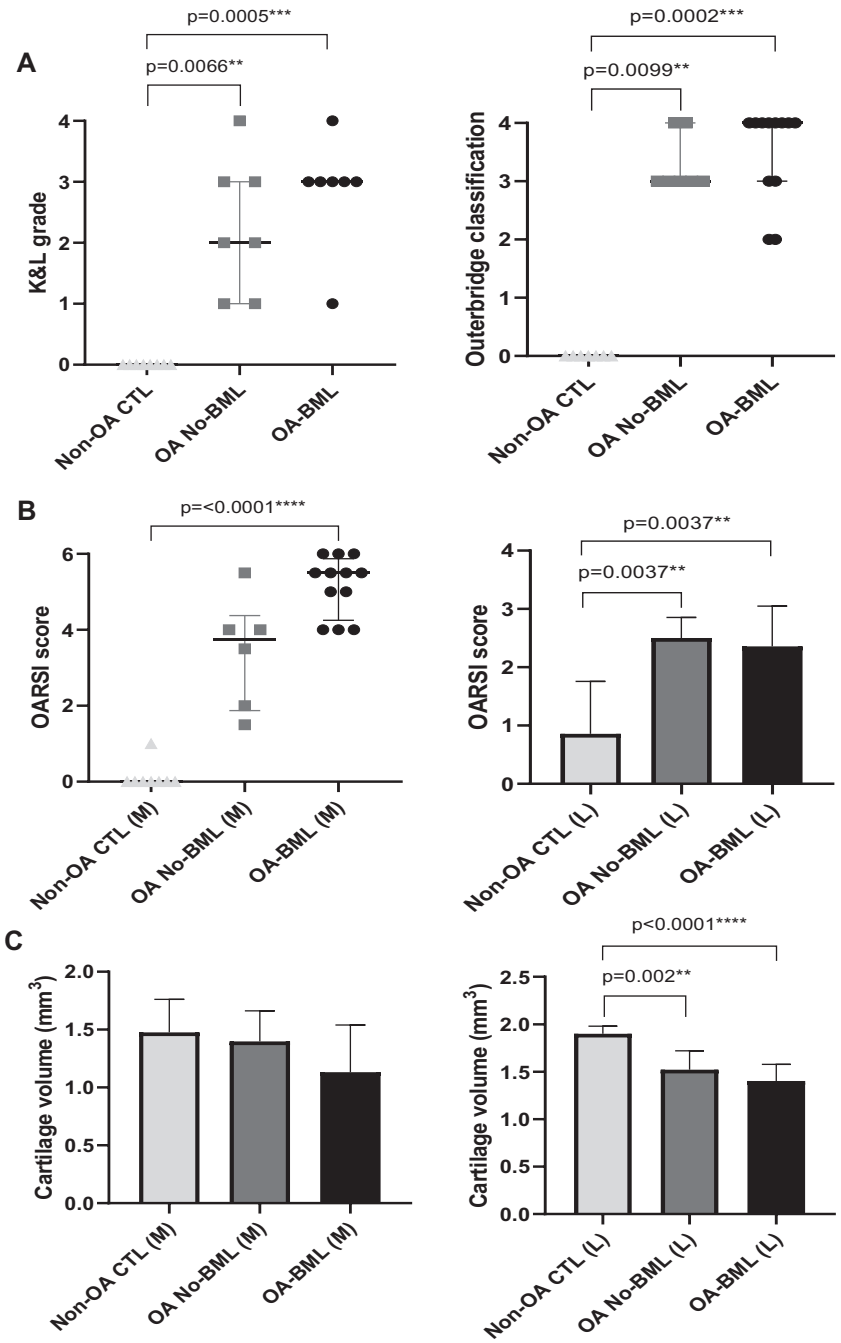

Fig. 2. (A) Radiographic K&L grade (of the whole TP), and macroscopic Outerbridge classification (of the whole TP) are presented as median (25th, 75th percentiles) and (B) microscopic OARSI score (sub-sampled for medial and lateral) are presented as median (25th, 75th percentiles) for medial and mean ± standard deviation for lateral, and (C) cartilage volume (mm^3) (sub-sampled for medial and lateral) are presented as mean ± standard deviation; p value < 0.05 was considered to be statistically significant.

3.3. Raman assessment (integrated area ratios)

3.3.1. Group comparison (within compartment)

The mineral:matrix integrated area ratio of Phosphate (v1):Amide III was significantly lower for OA-BML compared to Non-OA CTLs ($p = 0.04$) in the medial compartment (Fig. 5-A); with no group differences for the lateral compartment. No significant differences were observed for Carbonate:Phosphate (v2) between groups for either the medial or lateral compartment (refer to supplementary data table).

3.3.2. Medial-lateral comparisons

Significantly lower mineral:matrix integrated area ratio of Phosphate (v1 and v2):Amide III was found in the medial compartment compared to the lateral compartment for OA-BML ($p = 0.023$, $p = 0.009$; respectively) (Fig. 5-B). No other differences were observed.

4. Discussion

In this study we applied Raman microspectroscopy to investigate the material and biochemical composition properties of SCTB within BML zones of the TP in human knee OA. The main finding of our study was the reduced ratio of bone mineral:bone organic matrix in trabecular bone in BML zones of the medial TP for individuals with knee OA, compared with the same regions in TP without OA. Our study extends

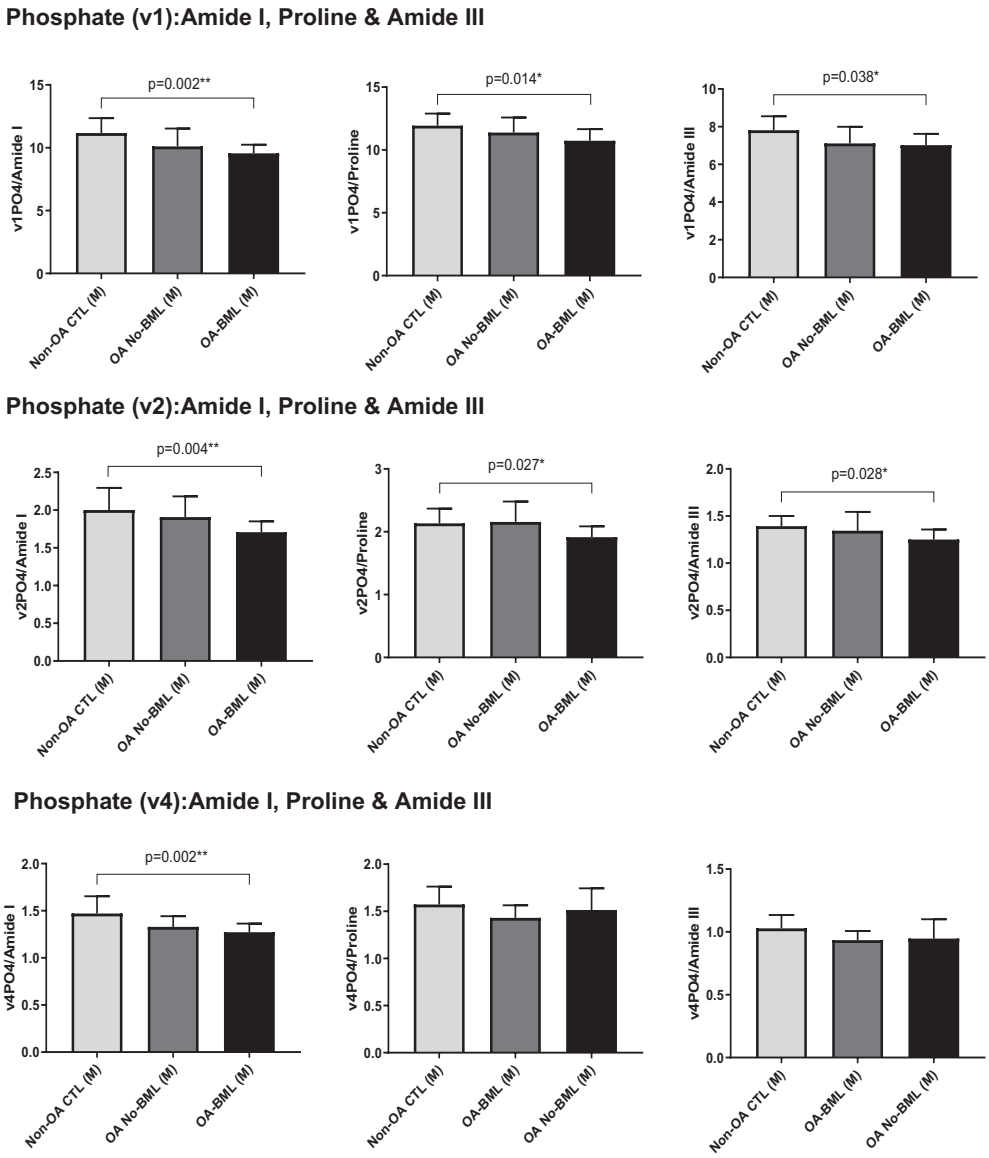

Fig. 3. The mineral:matrix peak ratios of Phosphate (v1, v2 and v4):Amide I, Proline and Amide III, within the medial compartment only, showing mean ± standard deviation; p values < 0.05 were considered to be statistically significant.

the earlier work of Kerns et al. (Kerns et al., 2014), which used Raman to investigate the biochemical properties of tibial SCTB in OA, but without consideration of the presence or absence of BMLs. Those authors were able to discriminate between OA bone and Non-OA CTL bone, on the basis of their Raman spectra, from either the medial or lateral SCTB compartment. Because the medial compartment typically contained more damaged cartilage, while the Raman signals were similar on both sides (unlike our study), they considered that bony changes precede cartilage degradation and loss or, intriguingly, that inherent differences exist in the OA bone. Also unlike our study, Kerns et al. reported increased mineralization of the subchondral bone (Phosphate:Amide I ratio) in the OA samples, compared with the controls. The reason for these different findings is unknown, but could relate to the presence or absence of BMLs in the tissue, different patient populations, or different sample handling and instrumentation settings. Since multiple spectral peaks in our study demonstrated lower Phosphate:Amide ratios, we are confident that our study supports the notion of reduced mineralization in BMLs compared with control subchondral tibial bone. Our results are consistent with the reported reduced mineralization in OA bone in general, and OA bone with BMLs, as demonstrated by other techniques, especially FTIR (Kazakia et al., 2013). Li and Aspen found reduced 'material density' in g/cm^3 for trabeculae in the femoral neck of OA individuals (Li and Aspden, 1997). Reduced mineralization is also consistent with earlier reports of OA subchondral bone (Day et al., 2001), and is associated with changes in collagen structure or amount in OA (Li and Aspden, 1997; Couchourel et al., 2009), and reduced elastic modulus (Day et al., 2001) and mechanical strength of the subchondral bone (Mühlhofer et al., 2009; Bailey et al., 2004). As already noted, reduced mineralization was reported in subchondral bone corresponding to BML zones, when measured by micro-CT and FTIR analysis (Kazakia et al., 2013; Hunter et al., 2009). Finally, our Raman data are supported by similar findings when we used electron back-scatter analysis of bone mineralization density distribution in BMLs (Kuliwaba et al., 2019).

Our data showed a significant decrease in the bone mineralization within the OA-BML zones compared to Non-OA CTLs, in the medial compartment. Since most BMLs occur on the medial side in KOA, we chose to examine only medial BMLs. The ratios of Phosphate (v1, v2 and v4): Amide I, Proline and Amide III, and the integrated area ratio of Phosphate (v1 and v2):Amide III were all lower within the OA-BML

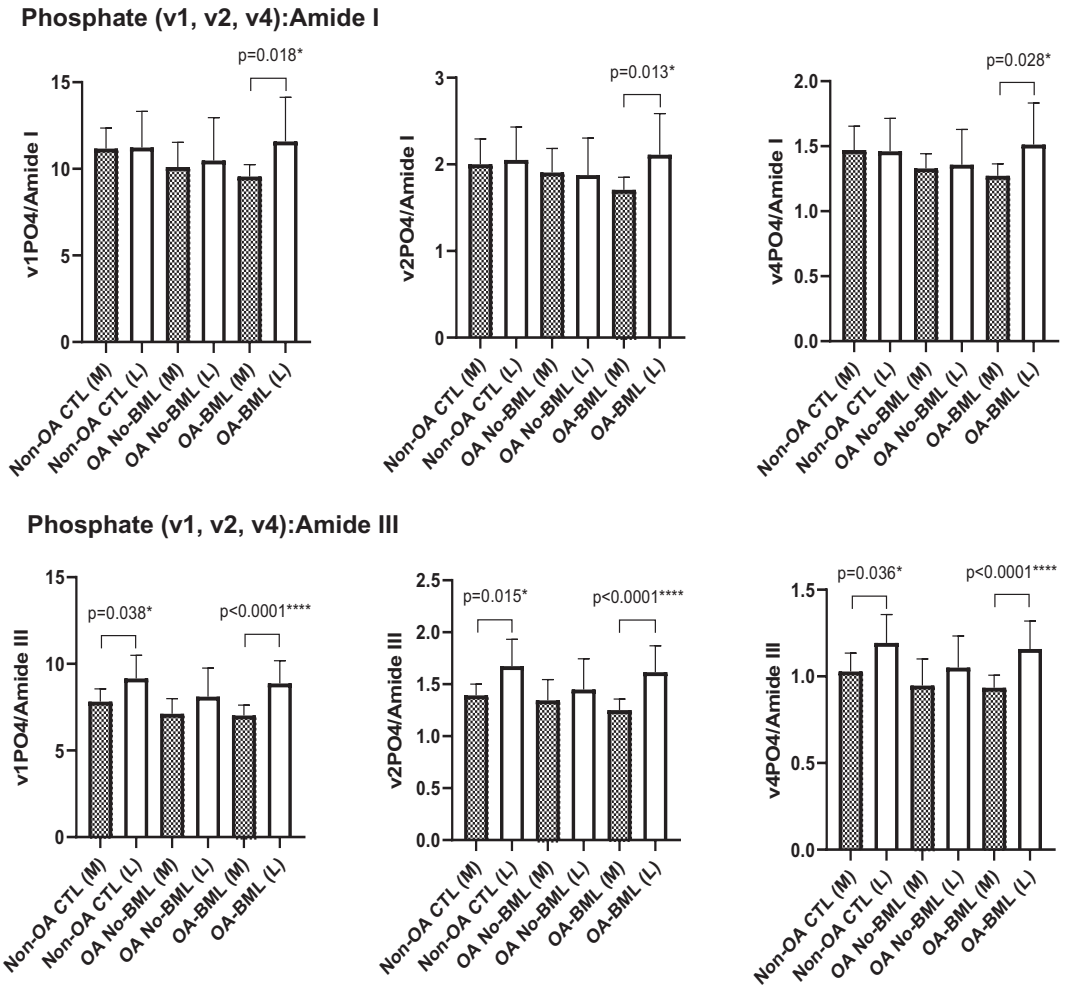

Fig. 4. The mineral:matrix peak ratios of Phosphate (v1, v2 and v4):Amide I and Amide III, for compartment differences in each group, showing mean ± standard deviation; p values < 0.05 were considered to be statistically significant.

trabecular bone compared to control bone from the corresponding sites. We interpret the data as demonstrating hypo-mineralization of the bone matrix within BMLs, and propose several possible causes for this effect. Firstly, hypo-mineralization could be due to an increased rate of bone remodeling in BMLs, consistent with our evidence of increased microdamage, eroded bone surface, and non-mineralized osteoid volume in BML bone (Muratovic et al., 2016, 2018, 2019; Burr and Gallant, 2012). Microdamage and repair may increase bone remodeling in individuals with OA and, collectively, our data suggest that BML areas of bone correspond to localized areas of active repair response and remodeling. Further, increased bone matrix microdamage and altered vasculature in the SCB of BMLs is consistent with overloading and vascular contributions to the formation of these lesions (Burr and Radin, 2003; Ruppel et al., 2006). Kazakia et al. used FTIR analysis to investigate BML zones as pulverized SCTB, and also reported reduced mineral:matrix ratios by that method (Kazakia et al., 2013). These authors obtained evidence of increased bone remodeling in these sites and also posited this as the cause for their observations (Kazakia et al., 2013).

Secondly, there is evidence that differential expression of collagen type I α1 and α2 chains results in matrix that is inherently a poorer substrate for mineralization in OA (Couchourel et al., 2009). Thus, *in vitro* studies have shown reduced mineralization by osteoblasts obtained from SCTB in OA (Couchourel et al., 2009) and this associated with an elevated *COL1A1:COL1A2* mRNA ratio, similar to the reported differential expression of these genes in OA human bone (Truong et al., 2006). Interestingly, in the light of more recent evidence for a direct role for TGFβ1 in the development of OA (Zhen et al., 2013), inhibiting TGFBβ1 in OA osteoblasts corrected the abnormal *COL1A1:COL1A2* ratio and increased cell mineralization (Couchourel et al., 2009).

A limitation of this study is that samples were collected from patients with late-stage knee OA, who presented for total joint replacement surgery, and therefore early SCTB tissue compositional changes of OA could not be observed. In addition, a relatively small number of samples were evaluated and further studies with a larger sample size are indicated.

In summary, our findings show the power of RS to interrogate fresh tissue samples of subchondral bone in OA, and other disease states. In this study, we showed that the mineral:matrix properties of OA-BML SCTB tissue are reduced when compared to Non-OA CTLs, consistent with demonstrations of hypo-mineralization of subchondral bone in OA, and particularly in BMLs, as obtained previously using other analytical methods. That OA-BML SCTB tissue has lower bone mineralization is perhaps related to active increased bone remodeling within BMLs. Changes in mineralization are likely to alter the biomechanical properties of the SCTB, with potential implications for the overlying cartilage. These findings further suggest the potential value of therapeutic targeting of the SCTB in OA.

Funding

The authors acknowledge funding from the National Health and Medical Research Council of Australia (NHMRC, Project Grant

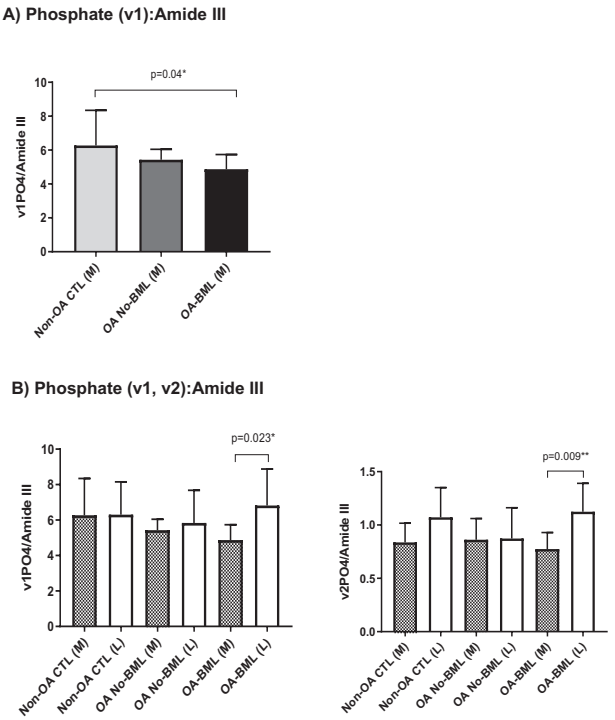

Fig. 5. The mineral:matrix integrated area ratio of (A) Phosphate (v1):Amide III, within the medial compartment only, and (B) Phosphate (v1 and v2):Amide III, for compartment differences in each group, are presented as mean ± standard deviation, with p values < 0.05 considered to be statistically significant.

1042482).

Authors' contribution

All authors meet the criteria for authorship, and approved the final paper. Y-RL contributed to the conception and design, acquisition of data, analysis, interpretation of data, drafting/revision of the paper. DMF contributed to the conception and design, interpretation of data and drafting/revision of the paper and funding of the project. DM contributed to the conception and design, collection of human specimens, acquisition of patients' demographic information, interpretation of MRI data and drafting/revisions of the paper. TKG contributed to statistical analyses and interpretation of data. JSK contributed to the conception and design, interpretation of data and drafting/revisions of the paper.

Transparency document

The Transparency document associated with this article can be found, in online version.

Declaration of competing interest

All authors declare that they have no conflict of interest regarding the work.

Acknowledgments

The authors wish to thank Dr Graham Mercer, Dr Chris Wilson, and Dr Dai Morgan for helping obtain TP specimens and performing Outerbridge classification; Ms Emma Giersch (EG) for OARSI scoring; Prof Anita Wluka (AW) and Dr Yuan-Yuan Wang (Y-YW) for K&L grading; and Dr Jamie Taylor for assistance and advice on measurement and interpretation of the radiographic and MRI data. The authors also wish to acknowledge support from the Department of Radiology at the Royal Adelaide Hospital and SA Tissue Bank, SA Pathology.

Appendix A. Supplementary data

Supplementary data to this article can be found online at https://doi.org/10.1016/j.bonr.2020.100269.

References

Awonusi, A., Morris, M.D., Tecklenburg, M.M., 2007. Carbonate assignment and calibration in the Raman spectrum of apatite. Calcif. Tissue Int. 81 (1), 46–52.
Bachra, B.N., Fischer, H.R., 1968. Mineral deposition in collagen in vitro. Calcif. Tissue Res. 2 (4), 343–352.
Bailey, A.J., et al., 2004. Biochemical and mechanical properties of subchondral bone in osteoarthritis. Biorheology 41 (3–4), 349–358.
Buchwald, T., et al., 2012. Identifying compositional and structural changes in spongy and subchondral bone from the hip joints of patients with osteoarthritis using Raman spectroscopy. J. Biomed. Opt. 17 (1), 017007.
Buckley, K., Matousek, P., Parker, A.W., Goodship, A.E., 2012. Raman spectroscopy reveals differences in collagen secondary structure which relate to the levels of mineralisation in bones that have evolved for different functions. Journal of Raman Spectroscopy 43 (9), 1237–1243.
Burr, D.B., Gallant, M.A., 2012. Bone remodelling in osteoarthritis. Nat. Rev. Rheumatol. 8 (11), 665–673.
Burr, D.B., Radin, E.L., 2003. Microfractures and microcracks in subchondral bone: are they relevant to osteoarthrosis? Rheum. Dis. Clin. N. Am. 29 (4), 675–685.
Butler, H.J., et al., 2016. Using Raman spectroscopy to characterize biological materials. Nat. Protoc. 11 (4), 664–687.
Couchourel, D., et al., 2009. Altered mineralization of human osteoarthritic osteoblasts is attributable to abnormal type I collagen production. Arthritis Rheum. 60 (5), 1438–1450.
Day, J.S., et al., 2001. A decreased subchondral trabecular bone tissue elastic modulus is associated with pre-arthritic cartilage damage. J. Orthop. Res. 19 (5), 914–918.
Dehring, K.A., et al., 2006. Identifying chemical changes in subchondral bone taken from murine knee joints using Raman spectroscopy. Appl. Spectrosc. 60 (10), 1134–1141.
Driban, J.B., et al., 2013. Evaluation of bone marrow lesion volume as a knee osteoarthritis biomarker—longitudinal relationships with pain and structural changes: data from the osteoarthritis initiative. Arthritis Res. Ther. 15 (5), R112.
Esmonde-White, K., 2014. Raman spectroscopy of soft musculoskeletal tissues. Appl. Spectrosc. 68 (11), 1203–1218.
Felson, D.T., et al., 2001. The association of bone marrow lesions with pain in knee osteoarthritis. Ann. Intern. Med. 134 (7), 541–549.
Felson, D.T., et al., 2003. Bone marrow edema and its relation to progression of knee osteoarthritis. Ann. Intern. Med. 139 (5 Pt 1), 330–336.
Frushour, B.G., Koenig, J.L., 1975. Raman scattering of collagen, gelatin, and elastin. Biopolymers 14 (2), 379–391.
Gamsjaeger, S., et al., 2010. Cortical bone composition and orientation as a function of animal and tissue age in mice by Raman spectroscopy. Bone 47 (2), 392–399.
Hunter, D.J., et al., 2006. Increase in bone marrow lesions associated with cartilage loss: a longitudinal magnetic resonance imaging study of knee osteoarthritis. Arthritis Rheum. 54 (5), 1529–1535.
Hunter, D.J., et al., 2009. Bone marrow lesions from osteoarthritis knees are characterized by sclerotic bone that is less well mineralized. Arthritis Res. Ther. 11 (1), R11.
Imbert, L., et al., 2014. Mechanical and mineral properties of osteogenesis imperfecta human bones at the tissue level. Bone 65, 18–24.
Ip, S., et al., 2011. Frequency of bone marrow lesions and association with pain severity: results from a population-based symptomatic knee cohort. J. Rheumatol. 38 (6), 1079–1085.
Kazakia, G.J., et al., 2013. Bone and cartilage demonstrate changes localized to bone marrow edema-like lesions within osteoarthritic knees. Osteoarthr. Cartil. 21 (1), 94–101.
Kazanci, M., et al., 2006. Bone osteonal tissues by Raman spectral mapping: orientation-composition. J. Struct. Biol. 156 (3), 489–496.
Kerns, J.G., et al., 2014. Evidence from Raman spectroscopy of a putative link between inherent bone matrix chemistry and degenerative joint disease. Arthritis Rheum. 66 (5), 1237–1246.
Kuhar, N., et al., 2018. Challenges in application of Raman spectroscopy to biology and materials. RSC Adv. 8 (46), 25888–25908.
Kuliwaba, J.S., et al., 2019. Biochemical profiling of bone marrow lesions in knee osteoarthritis patients: altered mineralization of the subchondral bone matrix. Osteoarthr. Cartil. 27, S111.
Lastra Luque, P., et al., 2019. Characterization of carbonate fraction of the Atlantic bluefin tuna fin spine bone matrix for stable isotope analysis. PeerJ 7, e7176.
Li, B., Aspden, R.M., 1997. Material properties of bone from the femoral neck and calcar femorale of patients with osteoporosis or osteoarthritis. Osteoporos. Int. 7 (5), 450–456.
Makowski, A.J., et al., 2013. Polarization control of Raman spectroscopy optimizes the assessment of bone tissue. J. Biomed. Opt. 18 (5), 55005.
Mandair, G.S., Morris, M.D., 2015. Contributions of Raman spectroscopy to the understanding of bone strength. Bonekey Rep. 4, 620.

Mansell, J.P., Bailey, A.J., 1998. Abnormal cancellous bone collagen metabolism in osteoarthritis. J. Clin. Invest. 101 (8), 1596–1603.
Morris, M.D., Mandair, G.S., 2011. Raman assessment of bone quality. Clin. Orthop. Relat. Res. 469 (8), 2160–2169.
Movasaghi, Z., Rehman, S., Rehman, I.U., 2007. Raman spectroscopy of biological tissues. Appl. Spectrosc. Rev. 42 (5), 493–541.
Mühlhofer, H., et al., 2009. Mineralisation and mechanical strength of the subchondral bone plate of the inferior tibial facies. Surg. Radiol. Anat. 31 (4), 237–243.
Muratovic, D., et al., 2016. Bone marrow lesions detected by specific combination of MRI sequences are associated with severity of osteochondral degeneration. Arthritis Res. Ther. 18, 54.
Muratovic, D., et al., 2018. Bone matrix microdamage and vascular changes characterize bone marrow lesions in the subchondral bone of knee osteoarthritis. Bone 108, 193–201.
Muratovic, D., et al., 2019. Bone marrow lesions in knee osteoarthritis: regional differences in tibial subchondral bone microstructure and their association with cartilage degeneration. Osteoarthr. Cartil. 27 (11), 1653–1662.
Nyman, J.S., et al., 2011. Measuring differences in compositional properties of bone tissue by confocal Raman spectroscopy. Calcif. Tissue Int. 89 (2), 111–122.
Pascart, T., et al., 2017. Region specific Raman spectroscopy analysis of the femoral head reveals that trabecular bone is unlikely to contribute to non-traumatic osteonecrosis. Sci. Rep. 7 (1), 97.
Pavlou, E., et al., 2018. Raman spectroscopy for the assessment of osteoarthritis. Ann. Joint 3.
Penel, G., et al., 2005. Composition of bone and apatitic biomaterials as revealed by intravital Raman microspectroscopy. Bone 36 (5), 893–901.
Raynauld, J.P., et al., 2008. Correlation between bone lesion changes and cartilage volume loss in patients with osteoarthritis of the knee as assessed by quantitative magnetic resonance imaging over a 24-month period. Ann. Rheum. Dis. 67 (5), 683–688.
Roberts, B.C., et al., 2018. Relationships between in vivo dynamic knee joint loading, static alignment and tibial subchondral bone microarchitecture in end-stage knee osteoarthritis. Osteoarthr. Cartil. 26 (4), 547–556.
Roschger, A., et al., 2014. Relationship between the v(2)PO(4)/amide III ratio assessed by Raman spectroscopy and the calcium content measured by quantitative backscattered electron microscopy in healthy human osteonal bone. J. Biomed. Opt. 19 (6), 065002.
Ruppel, M.E., Burr, D.B., Miller, L.M., 2006. Chemical makeup of microdamaged bone differs from undamaged bone. Bone 39 (2), 318–324.
Slattery, C., Kweon, C.Y., 2018. Classifications in brief: outerbridge classification of chondral lesions. Clin. Orthop. Relat. Res. 476 (10), 2101–2104.
de Souza, R.A., et al., 2012. Influence of creatine supplementation on bone quality in the ovariectomized rat model: an FT-Raman spectroscopy study. Lasers Med. Sci. 27 (2), 487–495.
Truong, L.H., et al., 2006. Differential gene expression of bone anabolic factors and trabecular bone architectural changes in the proximal femoral shaft of primary hip osteoarthritis patients. Arthritis Res. Ther. 8 (6), R188.
Turunen, M.J., et al., 2011. Comparison between infrared and Raman spectroscopic analysis of maturing rabbit cortical bone. Appl. Spectrosc. 65 (6), 595–603.
Unal, M., et al., 2018. Assessing glycation-mediated changes in human cortical bone with Raman spectroscopy. J. Biophotonics 11 (8), e201700352.
Waldstein, W., et al., 2016. OARSI osteoarthritis cartilage histopathology assessment system: a biomechanical evaluation in the human knee. J. Orthop. Res. 34 (1), 135–140.
Zhen, G., et al., 2013. Inhibition of TGF-beta signaling in mesenchymal stem cells of subchondral bone attenuates osteoarthritis. Nat. Med. 19 (6), 704–712.